Li-ion battery separator membranes based on barium titanate and poly(vinylidene fluoride-co-trifluoroethylene): Filler size and concentration effects

J. Nunes-Pereira [a], C.M. Costa [a], R.E. Sousa [a], A.V. Machado [b], M.M. Silva [c], S. Lanceros-Méndez [a,*]

[a] Centro/Departamento de Física, Universidade do Minho, 4710-057 Braga, Portugal

[b] Departamento de Engenharia de Polímeros, Universidade do Minho, 4800-058 Guimarães, Portugal

' Centro/Departamento de Química, Universidade do Minho, 4710-057 Braga, Portugal

Keywords:

Porous membranes
Barium titanate
Poly(vinylidene
fluoride-co-trifluoroethylene)
Lithium ion batteries and size effect

Abstract

Microporous polymer membranes based on poly(vinylidene fluoride-co-trifluoroethylene)(P(VDF-TrFE)) with barium titanate ($BaTiO_3$) ceramic nanoparticles at different concentration (4,16 and 32%) and average sizes (10,100 and 500 nm) were prepared by thermally induced phase separation. The effects of fillers concentration and size on morphological, thermal, mechanical and electrochemical properties were evaluated. Pores remain homogeneously distributed after the addition of the fillers. In turn, the average pore size increases from $\sim 25\mu$ m for the pristine polymer to 90μ m for the membrane with 32wt% of $BaTiO_3$. The porosity, on the other hand, remains nearly constant at $\sim$ 72%. The ionic conductivity increases in all temperature range with the addition of $BaTiO_3$, being this increase larger for samples

prepared with larger diameter filler particles. The stable operation window is at least 6.0 V for all membranes.

It was concluded that morphological, mechanical and electrochemical properties of the $BaTiO_3$ filled P(VDF-TrFE) membranes actually depend on filler size and concentration the most adequate membrane for battery separator applications being the $BaTiO_3/P(VDF-TrFE)$ membrane with 16wt% of 500 nm diameter ceramic fillers.

Introduction

Current lifestyle and technological advances, in particular in the area of mobile communications, lead to an increased need and availability of stored energy [1,2]. Despite the many emerging technologies, the most attractive way to store energy to provide electrical power is to convert chemical into electrical energy. In this sense, lithium ion secondary batteries are the systems with the best performance with higher working voltage and energy density (210 Wh/kg; 650 Wh/l), longer service life and higher flexibility design when compared to other systems such as lead-acid, $Ni-Cd$ or $Ni-MH$ batteries [1-4].

Up to know, the development of lithium secondary batteries has been mostly focused on powering small electronic devices, but new developments are needed to meet the requirements of new market trends, such as green energy, recycling and flexibility, among

others. One way to accomplish these requirements is the use of polymers or organic/inorganic composites [2].

A battery is a device that converts stored chemical energy into electricity within a closed system. Lithium ion batteries have three fundamental constituents, the negative electrode (anode), the positive electrode (cathode) and the electrolyte within a separator. Most Li-batteries use carbon as anode, metal oxides as cathode and organic solvents as electrolyte solutions [2,5]. The separator is often a porous polymer or ceramic membrane placed between cathode and anode. It plays a key role in the battery performance and safety, providing electrical insulation between electrodes and a pathway for ionic conduction. An ideal separator should meet requirements such as being electronic insulator, ionic conductor, mechanically strong, dimensionally stable, readily wetted by electrolyte and chemically resistant to electrolyte and impurity degradation, among others [2,5,6]. Many polymers meet these demands and therefore many studies have been developed for their use as separators: poly(ethylene oxide) (PEO) [7-10], poly(acrylonitrile) (PAN) [11,12], polyimide (PI) [13] and poly(vinylidene fluoride) (PVDF) and its copolymers [14-20].

PVDF and poly(vinylidene fluoride-co-trifluoroethylene) (P(VDF-TrFE)) have attracted interest as battery separator due to

Table 1
Structural properties of the ceramic fillers [34].

	$\phi = 10$ nm	$\phi = 100$ nm	$\phi = 500$ nm
Purity (%)	99.8	99.9	99.9
Crystallographic form	cubic	cubic	tetragonal

its large polarity, controllable porosity, suitable mechanical properties, wettability by organic solvents, chemically inertness, good electrode/electrolyte contact and stability in cathodic environment [14,15,21,22].

In particular, P (VDF-TrFE) has high polarity and crystallizes in a polar phase from the melt or by solution casting and its ferroelectric to paraelectric transition (FE-PE) occurs at a temperature (T_c) below the melting temperature (T_m) [23].

Despite the advances in the development in polymer based separator membranes, there is still large space for improvement. In this way, the incorporation of suitable fillers in polymer matrixes has become an interesting approach to improve mechanical, thermal and chemical stability and electrolyte uptake of the separators. The use of carbon nanotubes [24], zeolites [22], clays [21,25], barium titanate ($BaTiO_3$) [26-28] and others have been recently reported. Ferroelectric ceramic fillers, as $BaTiO_3$, enhance lithium interface stability, facilitate the salt dissociation into charge species and improve the ionic conductivity, by increasing the amorphous phase content of the polymers and the number of charge carriers [27].
$BaTiO_3$ crystallizes in the perovskite structure [29] and has high dielectric response at room temperature ($\varepsilon = 1200, \Phi = 10$ nm; $\varepsilon = 3417, \Phi = 500$ nm)[30,31]. $BaTiO_3$ exhibits five crystalline phases, hexagonal, cubic, tetragonal, orthorhombic, monoclinic and rhombohedral depending on temperature [32].

Recent studies report on the use of polymeric composites with $BaTiO_3$ as separator membranes. The addition of this ceramic filler in a PEO/P(VDF-TrFE) polymer blend increases the ionic conductivity up to 1.2×10^{-4} S/cm and the stable operation window to a range of -2.3 to 2.4 V for 15wt% of $BaTiO_3$ [26]. Composites of PEO with $BaTiO_3$ also show high ionic conductivity, 1.5×10^{-5} S/cm, at room temperature, and a stable operation window up to 4.1 V vs Li/Li^+ at 80°C for 10wt% of fillers [28].

The successful use of the ferroelectric filler $BaTiO_3$ reinforce the relevance of this work, since besides the effect of filler content, the effect of filler size in the morphological, thermal, mechanical, electrochemical properties of the polymeric membranes is also considered. This fact is relevant and the $BaTiO_3$ particle properties and therefore their effect in a composite highly depend on particle size, the ferroelectricity disappearing below a certain grain size [33]. In this study particles of 10, 100 and 500 nm average size are evaluated.

Experimental Details

Materials

Poly(vinylidene fluoride trifluorethylene) (P(VDF-TrFE)) (70/30) was acquired from Solvay and barium titanate particles ($BaTiO_3$) with average size of 10,100 and 500 nm were obtained from Nanoamor, with the characteristics summarized in Table 1. Propylene carbonate (PC) and Lithium perchlorate trihydrat ($LiClO_4 \cdot 3H_2O$) were acquired from Merck.

Membrane preparation

$BaTiO_3$/P(VDF-TrFE) membranes were prepared by dispersing the ceramic nanoparticles in a solution of N, N-dimethylformamide (DMF, from Merck) in an ultrasonic bath during 4 hours. The polymer was added to the solution to obtain a concentration of 15% (w/w). The ceramic particles to polymer relative concentrations ranged from 0 up to 32%$BaTiO_3$ content (w/w). The solution was prepared at room temperature with the help of a magnetic stirrer until complete polymer dissolution, i.e., until a homogeneous and transparent solution was obtained (~ 2 hours). In order to prevent the formation of aggregates and to improve polymer dissolution, the solution temperature was increased 5°C above room temperature during the first 15 min . Finally, the mixture was placed in a glass Petri dish and the DMF solvent completely evaporated at room temperature during 15 days in a gas extraction chamber.

Electrolyte solution and uptake

The electrolyte solution uptake was performed immersing the membranes in an electrolyte solution of $1MLiClO4.3H_20$ in PC for 24 hours.

The electrolyte content ($E_{content}$) was evaluated according to:

$$E_{content} = 1 - \frac{m_0}{m_E} \times 100 \quad (1)$$

where $\mathbf{m_0}$ is the mass of the dry membrane and $\mathbf{m_E}$ is the mass of the membrane filled with electrolyte solution. $LiClO_4.3H_20$ was chosen for the electrolyte solution as it improves the conductivity of the composite as compared to $LiClO_4$ [15,35].

Characterization techniques

Membranes were coated with a thin gold layer using a sputter coating (Polaron, model SC502 sputter coater) and the morphology analyzed using a scanning electron microscope (SEM) (Leica Cambridge apparatus at room temperature). The average pore diameter was determined on the basis of the diameter of 40 pores, using the SEM images at 200x magnification and the Image J software.

The porosity of the membranes (ε) was measured with a pycnometer by the following procedure: the pycnometer was filled with ethanol and the mass was measured (m_1); the mass of the sample was measured (m_0) and then immersed in ethanol; after the sample being completely soaked in ethanol, more ethanol was added to fill completely the pycnometer, and the mass of the assembly (sample + pycnometer) was measured (m_2); finally, the sample was removed from the pycnometer and the residual weight of the pycnometer with ethanol was measured (m_3). Ethanol was used because of its low density and easy soaking within the sample.

The porosity of the membrane was calculated according to:

$$\varepsilon = \frac{m_2 - m_3 - m_0}{m_1 - m_3} \quad (2)$$

The mean porosity of each membrane was obtained as the average of the values determined in six measurements.

Polymer phase in the composites was evaluated by Fourier Transformed Infrared Spectrostopy (FTIR) performed at room temperature with a Jasco FT/IR-4100. FTIR spectra were collected in the ATR mode from 4000 to 600 cm^{-1} after 32 scans with a resolution of 4 cm^{-1}.

The thermal properties of the composites were determined by differential scanning calorimetry (DSC) with a Mettler Toledo 821^e apparatus. The samples were cut from the central region of the membranes, placed in 50μ L crucibles and heated from 50 to 200°C at a rate of 10°C/min, under an argon atmosphere. The degree of crystallinity (χ_c) was calculated (Eq. 3) from the melting/crystallization enthalpy (ΔH_f) based on the enthalpy of a 100% crystalline sample ($\Delta H_{100} = 103.4$ J/g) [36]:

$$\chi_c = \frac{\Delta H_f}{\Delta H_{100}} \times 100 \tag{3}$$

The mechanical properties were evaluated by stress strain measurements carried out in a TST350 Linkam Scientific Instruments set up at a strain rate of 15μ m/s.

The ionic conductivity was evaluated by an Autolab PGSTAT-12 (Eco Chemie) set-up in a frequency range from 500 mHz to 65 kHz . The samples were placed in a constant volume support equipped with gold blocking electrodes located within a Buchi TO 50 oven. The temperature, measured by a type K thermocouple, was varied between 20 and 120°C. The ionic conductivity (σ_i) was calculated for each heating cycle according to:

$$\sigma_i = \frac{d}{R_b A} \tag{4}$$

where R_b is the bulk resistance, d is the thickness and A is the area of the sample.

The tortuosity (τ), the ratio between the effective capillarity and thickness of the sample was determined by:

$$\tau = \sqrt{\frac{\sigma_0 \varepsilon}{\sigma_i}} \tag{5}$$

where $\boldsymbol{\sigma_0}$ is the conductivity of the liquid electrolyte, $\boldsymbol{\sigma_i}$ is the conductivity of the membrane and the electrolyte set at room temperature and $\boldsymbol{\varepsilon}$ is the porosity of the membrane.

The ionic conductivity temperature dependence follows the Arrhenius equation:

$$\sigma_i = \sigma_0 \exp\left(\frac{-E_a}{RT}\right) \tag{6}$$

where $\boldsymbol{\sigma_0}$, is the pre-exponential factor, $\mathbf{E_a}$ is the apparent activation energy for ion transport, **R** is the gas constant (8.314 J/mol. K) and T is the temperature.

Cyclic voltammetry was performed within a glove box with argon atmosphere using a two electrode configuration and a gold microelectrode as working electrode. The 25μ m diameter gold microelectrodes were previously polished, washed with tetrahydrofuran (THF) and dried in hot air. The cell assembly was performed within the glove box by placing a lithium disk (10 mm diameter, 1 mm thick, Aldrich, 99.9% purity) as a counter electrode on a stainless steel current collector. Then the sample was centered over the counter electrode and the gold microelectrode was centered over the sample. The assembly was firmly attached by a clamp, placed inside a Faraday cage and connected to an Autolab PGSTAT-12 (Eco Chemie) that records the voltammograms at a scan rate from 0.05 to 1mV/s. From the voltammograms, the diffusion coefficient (D) of the electroactive species was calculated according to the Randles-Sevcik equation [37]:

$$i_p = (2.69 \times 10^5) n^{3/2} A D^{1/2} v^{1/2} C_0 \quad (7)$$

where $\mathbf{i_p}$ is the oxidative peak current in A, $\mathbf{n}$ is the number of electrons transferred in the redox reaction, $\mathbf{A}$ is the electrode area in cm^2, $\mathbf{v}$ is the potential scan rate in V/s and $\mathbf{C_0}$ is the analyte concentration in mol/cm^3.

Results and discussion

Microstructural characteristics

The effect of $BaTiO_3$ concentration in the polymer matrix was studied in the membranes with average particle size of 100 nm .

The morphology of the separator membrane is determinant in the performance of the battery as well as in their assembling and handling [5]. It has been shown that pristine P(VDF-TrFE) membranes produced under specific solvent evaporation conditions lead to porosity and pore distribution adequate for Li-ion batteries applications [14,38]. Prepared under those optimized conditions, Fig. 1 shows the cross section SEM pictures of P(VDF-TrFE) and P(VDFTrFE)/ceramic composites, and the average pore size distribution and electrolyte solution uptake for the sample with 16wt% filler content.

Fig. 1a, shows that the pristine copolymer is characterized by a homogeneous porous structure that remains after the addition of ceramic fillers (Fig. 1b c and d). In the inset of Fig. 1c and d it is notorious that the $BaTiO_3$ nanoparticles decorate the internal walls of the polymer pores, the fillers being located in the pore cavities instead of being incorporated within the polymeric matrix.

Fig. 1e represents the average pore size distribution of the sample with 16wt% of fillers, all the pores have a diameter between 40 and 70μ m. The average pore size for all samples is represented in Fig. 2.

Fig. 1f represents the electrolyte content as a function of time for the sample with 16wt% of $BaTiO_3$ nanoparticles. The electrolyte content stabilizes about 2 minutes after the onset. After stabilizing, the electrolyte content varies about 2%, which is within the experimental error. The behavior is similar for the remaining samples.

Fig. 2 shows the average pore size, porosity (Fig. 2a) and electrolyte content (Fig. 2b) of the different membranes.

Fig. 2a shows that the pore size increases with increasing $BaTiO_3$ content, between a minimum of $\sim 25\mu$ m for the pure polymer to a maximum $\sim 90\mu$ m for the composite with 32wt% of ceramic filler, which is to be ascribed to the filler effect on the bi-phase solventpolymer phase diagram and therefore on the phase separation and solvent evaporation processes [39]. On the other hand, the degree of porosity is not significantly affected, being the variations within experimental error.

Fig. 2b shows that the electrolyte content decreases with increasing ceramic nanoparticles content, between approximately 76 and 59%. Samples with higher amounts of fillers have less free space in the pore cavities for the electrolyte liquid, resulting in lower electrolyte content. Further, larger pore sizes for a given degree of porosity leads to lower surface area for interaction between separator and electrolyte.

The results of the weight loss proved to be negligible. Losses over 60 min time do not show any significant variation due to the high evaporation temperature ($242°C$) of the PC solvent of the electrolyte [40].

Polymer Phase and degree of crystallinity

Fig. 3 shows the infrared spectra of and the DSC thermogram for membranes with different filler contents.

The infrared spectra shows that the presence of the fillers does not affect the characteristic vibration modes ($851\ cm^{-1}, 886\ cm^{-1}$ and $1402\ cm^{-1}$) of the all-trans configuration of the polymer matrix [41]. The polymer crystallizes therefore in the polar phase after the addiction of $BaTiO_3$ ceramic particles. These characteristic vibration modes are also unaffected by the presence of electrolyte solution [21,22].

The thermograms of Fig. 3b show two endothermic peaks, the first around $117°C$, corresponding to the polymer ferroelectric to paraelectric transition (T_{FP}) and the second around $146°C$ corresponding to the polymer melting temperature (T_m) [42]. The addition of $BaTiO_3$ does not affect these reference temperatures of the polymer. In the presence of electrolyte solution these parameters are also unaffected by the fillers [21,22].

Table 2 shows the degree of crystallinity of the composite membranes calculated by eq. 3 .

The Table 3 shows that the degree of crystallinity of the composites membranes is lower than that of the pure polymer. The inclusion of fillers generally leads to a initial increase of the degree of crystallinity as small filler contents can act as nucleation agents

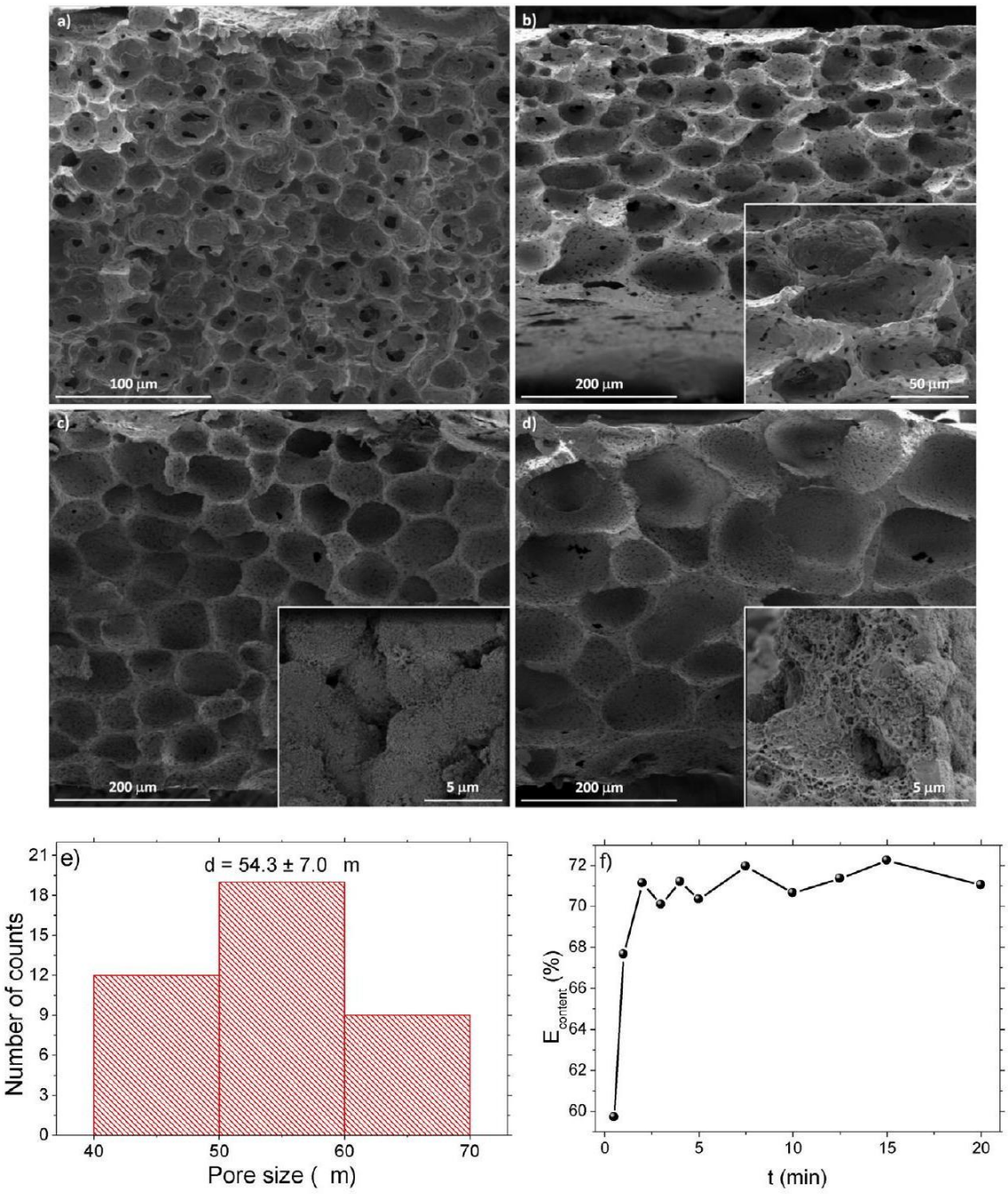

Fig. 1. Cross section SEM images of the $BaTiO_3$/P(VDF – TrFE) composites with different filler contents: a) 0wt%, b) 4wt%, c) 16wt% and d) 32wt%; e) average pore size distribution and f) electrolyte content as function of time, for membrane with 16wt% of $BaTiO_3$.

during the crystallization process. On the other hand, larger filler contents decrease the degree of crystallinity as ill crystallization of the polymer often occur in the presence of large content of ceramic fillers, that act as defects during the crystallization process [43].

Mechanical properties

Fig. 4 show the stress strain mechanical measurements for all the membranes after electrolyte solution uptake and the

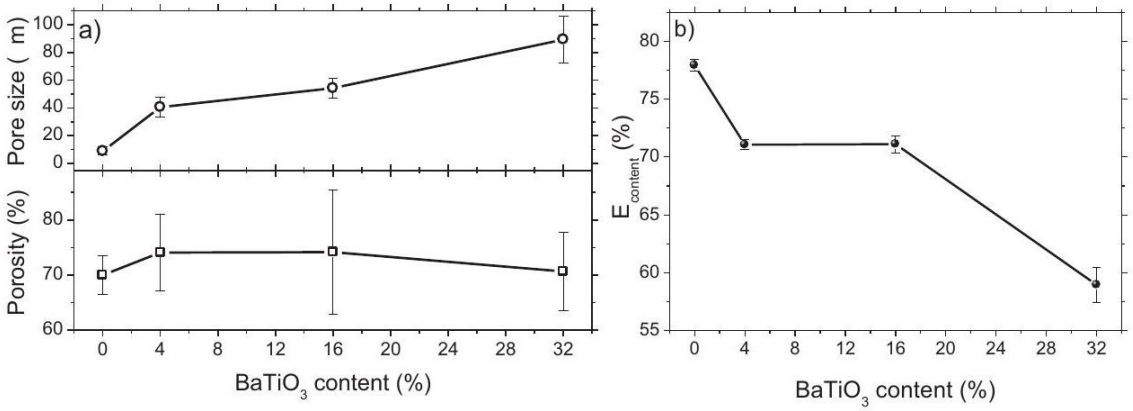

Fig. 2. a) Average pore size and porosity and b) electrolyte content as function of $BaTiO_3$ content for all membrane.

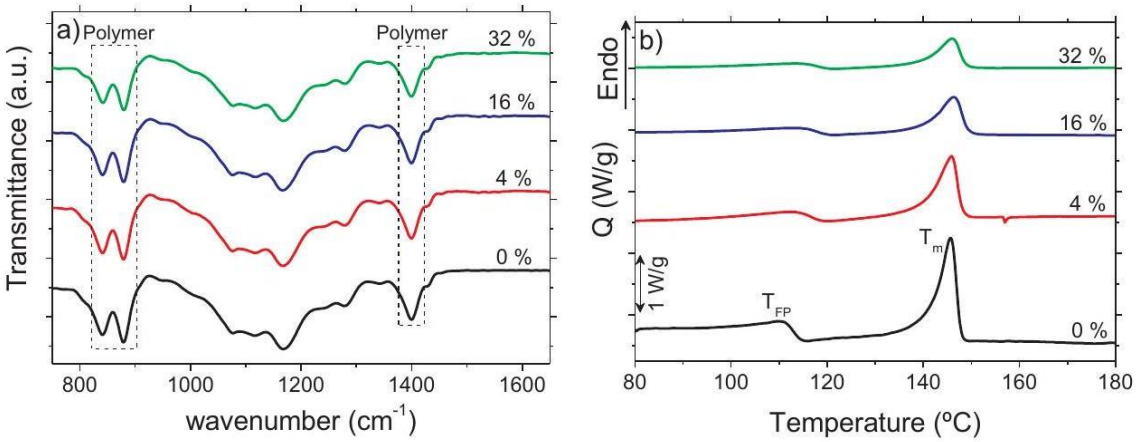

Fig. 3. a) FTIR spectra of the $BaTiO_3$/P (VDF-TrFE) composites with different filler contents; b) DSC thermogram of membrane composites with different amounts of ceramic particles.

Table 2
Degree of crystallinity of the $BaTiO_3/P(VDF - TrFE)$ membranes with different amounts of ceramic fillers.

Sample	χ_c(%)
0%	28
4%	29
16%	26
32%	20

Table
Mechanical properties of the membranes with electrolyte solution uptake.

Sample	Yield Stress (MPa)	Elastic Modulus (MPa)	Stress at break (MPa)
0%	0.3	1.9	1.0
4%	0.9	3.0	2.6
16%	0.7	2.8	2.0
32%	1.3	5.4	3.2

main parameters of the mechanical evaluation are summarized in Table 3.

The addition of $BaTiO_3$ to the polymer matrix affects the overall mechanical properties of the membranes. The yield stress, elastic modulus and stress at break show a slightly increase in the composites membranes when compared to the pure polymer, thus indicating that ceramic particles mechanically reinforce the composite despite the decrease in crystallinity of the polymeric matrix [43-45]. In this sense the mechanical reinforcement effect due to filler polymer interactions over impose any effect related to the variation in the degree of crystallinity. The proper wetting of the

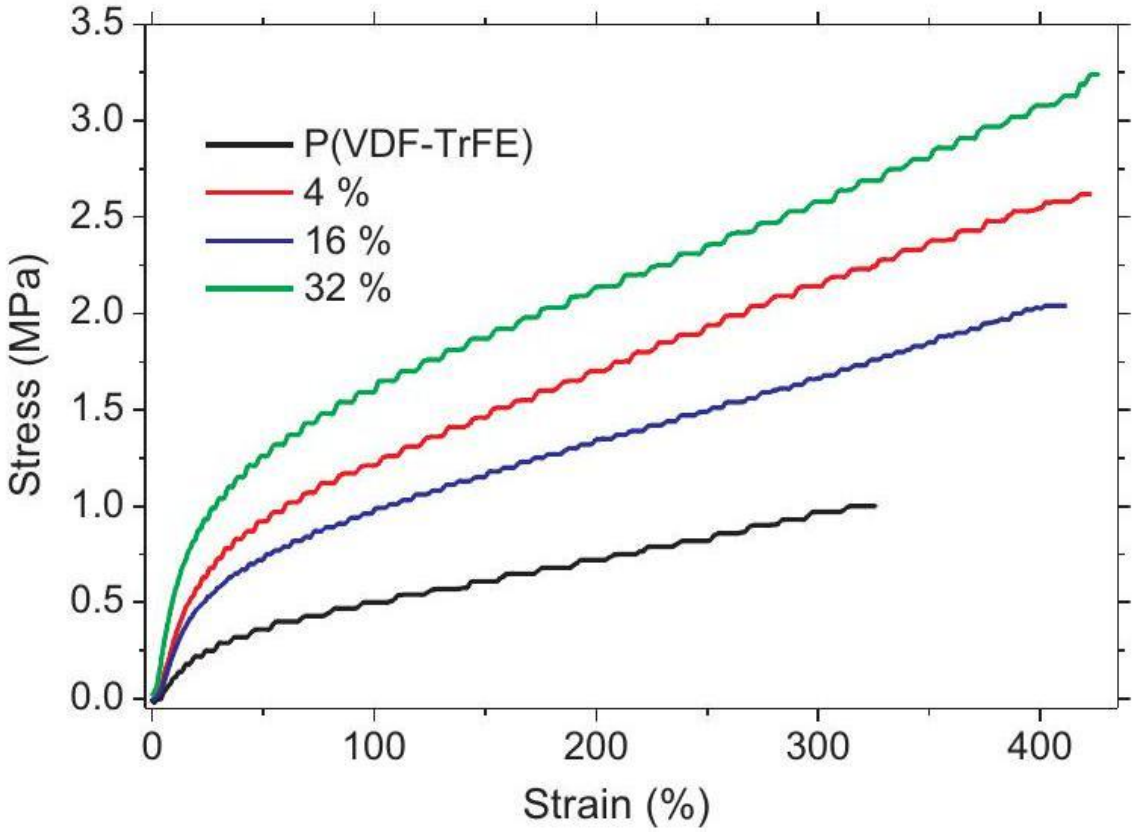

Fig. 4. Stress-strain curves of the $BaTiO_3$/P (VDF-TrFE) composites with different ceramic nanoparticles contents after electrolyte solution uptake.
ceramic filler by the polymer due to strong electrostatic interactions [43] lead to a mechanical reinforcement of the polymer within the composite, increasing the stress values needed for a given deformation. On the other hand, the overall mechanical properties remain in same value range, being therefore determined by the microporous microstructure of the membranes.

Electrical response

Impedance spectroscopy was performed to evaluate the electrochemical properties of the membranes with electrolyte solution uptake. The results are presented trough Nyquist plots (imaginary impedance Z" versus real impedance Z', Fig. 5a) and logarithmic ionic conductivity versus temperature (Fig. 5b).

Table 4 shows the ionic conductivity (σ_i) and tortuosity (τ) at room temperature, obtained from eq. 4 and 5 respectively.

The Nyquist plot is characterized by three distinct regions: a semicircle at high frequencies corresponding to the charge transfer process, a straight line at low frequencies is related to the diffusion process and the transition between both processes [46,47]. In the Nyquist plot of Fig. 5a, the high frequency semicircle appears only for the pristine polymer. It indicates that the fillers facilitate the charge transfer process due to the increase in ionic conductivity, as observed in Fig. 5b [48].

Fig. 5b represents the ionic conductivity as function of temperature for the different membranes with electrolyte uptake. The ionic conductivity of the composite membranes is about two orders of magnitude higher than for the pure polymer (Table 4), the ionic conduction is promoted by fillers through the increase of charge carriers and amorphous phase content in the composites (Fig. 3b and Table 2). Furthermore, in the composite membranes the ionic conductivity is more stable in temperature [45].

Regarding tortuosity, composites present substantially lower values than the pure polymer. The tortuosity gives information about pore connectivity relating the mean actual path with direct sample thickness and it is often defined trough the ionic conductivity [5]. Tortuosity of polymer composites is substantially lower than for the pure polymer, which indicates that the present of the fillers improve pore connectivity. The membrane with 4wt% of

Table 4
Room temperature ionic conductivity (σ_i) and tortuosity (τ) of the membranes filled with $1MLiClO4.3H_2O$ electrolyte solution; $\sigma_0 = 9.8mS/cm$ at 25°C.

Sample	σ_i(S/cm)	τ
0%	5.24×10^{-7}	114.9
4%	1.04×10^{-4}	8.4
16%	4.13×10^{-5}	13.4
32%	6.40×10^{-5}	10.4

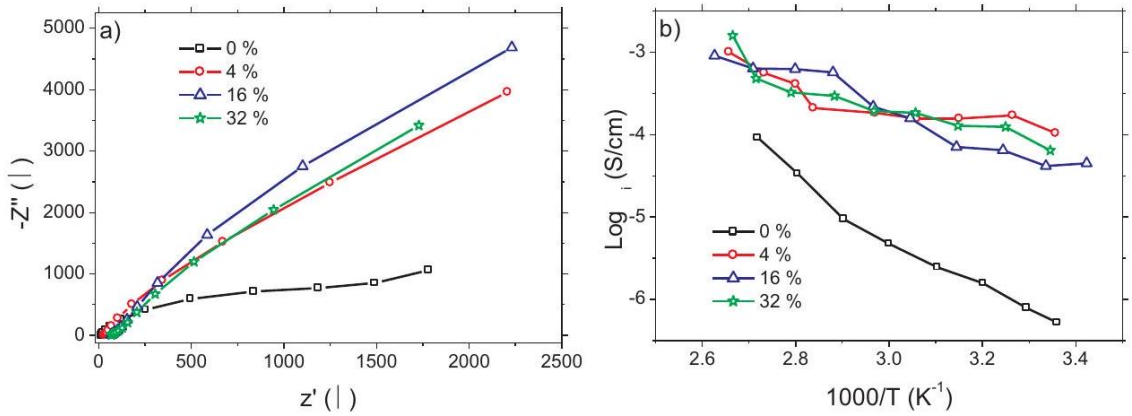

Fig. 5. a) Nyquist plot for the $BaTiO_3$/P(VDF-TrFE) composites at 25°C; b) log σ_i as a function of 1000/T for $BaTiO_3$/P(VDF-TrFE) composites with electrolyte solution uptake.

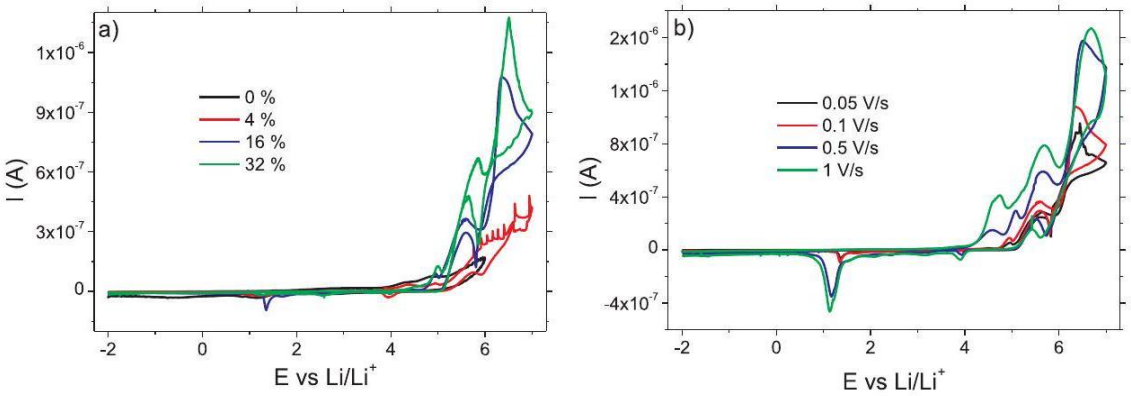

Fig. 6. a) Voltammogram of $BaTiO_3$/P(VDF – TrFE) composites at 0.1 V/s with different filler contents; b) voltammogram of $BaTiO_3$/P(VDF – TrFE) with 16wt% of ceramic particles with 100 nm in diameter at different scanning rates.

Table 5
Activation energy (E_a) of the composite membranes with electrolyte solution uptake, determined after eq. 6 .

Samples	E_a(kJ/mol)
0%	64
4%	11
16%	15
32%	10

$BaTiO_3$ shows the lower value of tortuosity, despite the differences between composite membranes being small, the obtained values suggest that for higher concentration pore

blockage occurs as well as interface trapping of ions. An ideal porous body has tortuosity of ~ 1, so the porous structure of composites is not far from the ideal value.

Table 5 represents the values of the activation energy of the conductive process.

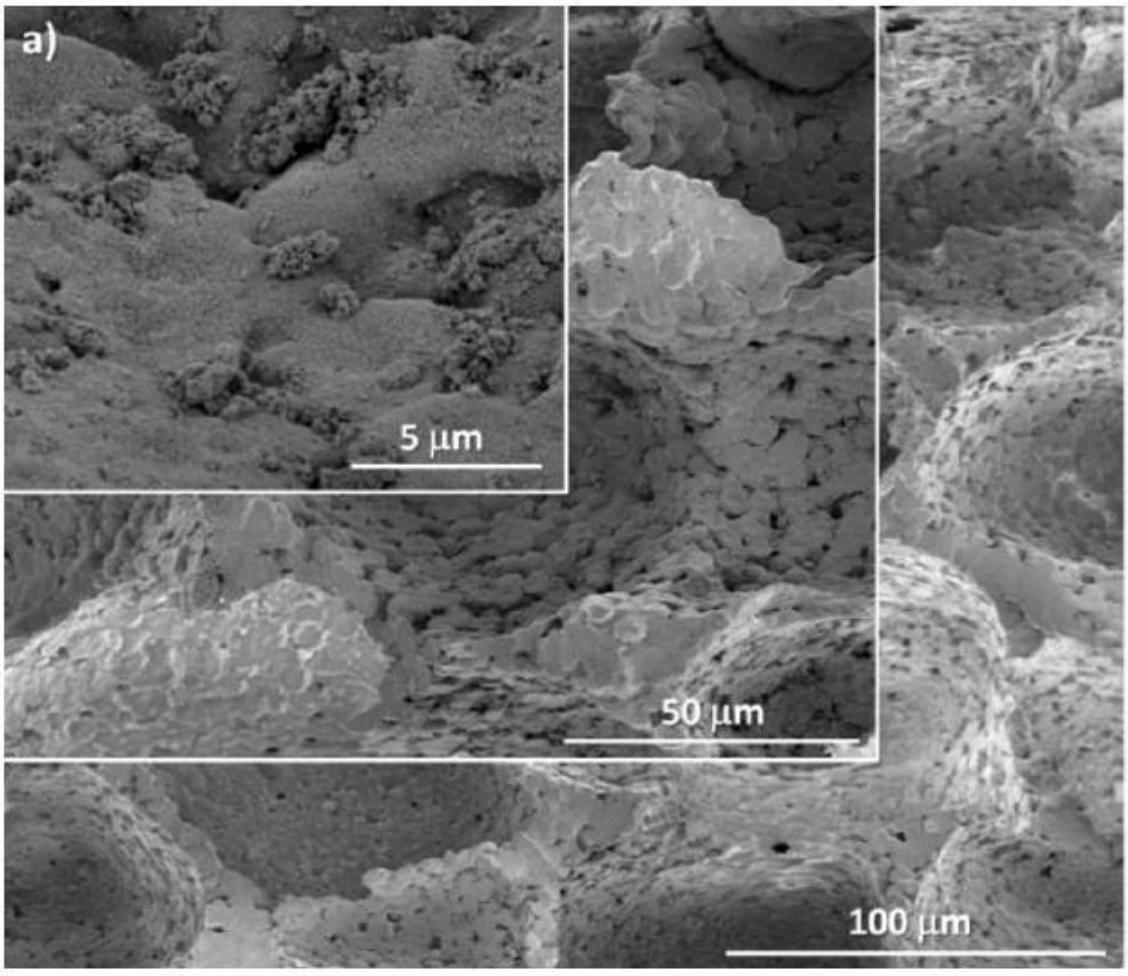

Table 5 shows that activation energy is lower and similar for all composite membranes, with respect to the pure polymer. The activation energy decreases substantially in composite membranes, which could be associated to the decrease of the degree of crystallinity and the increase in the number of charge carriers, which leads to an increase of the ionic mobility.

The Fig. 6 presents the cyclic voltammetry for samples with different $BaTiO_3$ contents (Fig. 6a) and scan rates (Fig. 6b) used to evaluate the electrochemical stability of the membranes.

The voltammograms of Fig. 6a show stable operation windows between - 2.0 and 4.0 V . The amount of fillers does not affect significantly the electrochemical stability, although composite membranes present a cathodic peak higher than the pure polymer around 6.0 V , probably due to charges accumulated at the interface between electrodes and sample [49]. The voltammograms of Fig. 6b also show stable operation windows between -2.0 and

4.0 V . For the higher scan rates, 0.5 and 1 V/s, an anodic peak appears

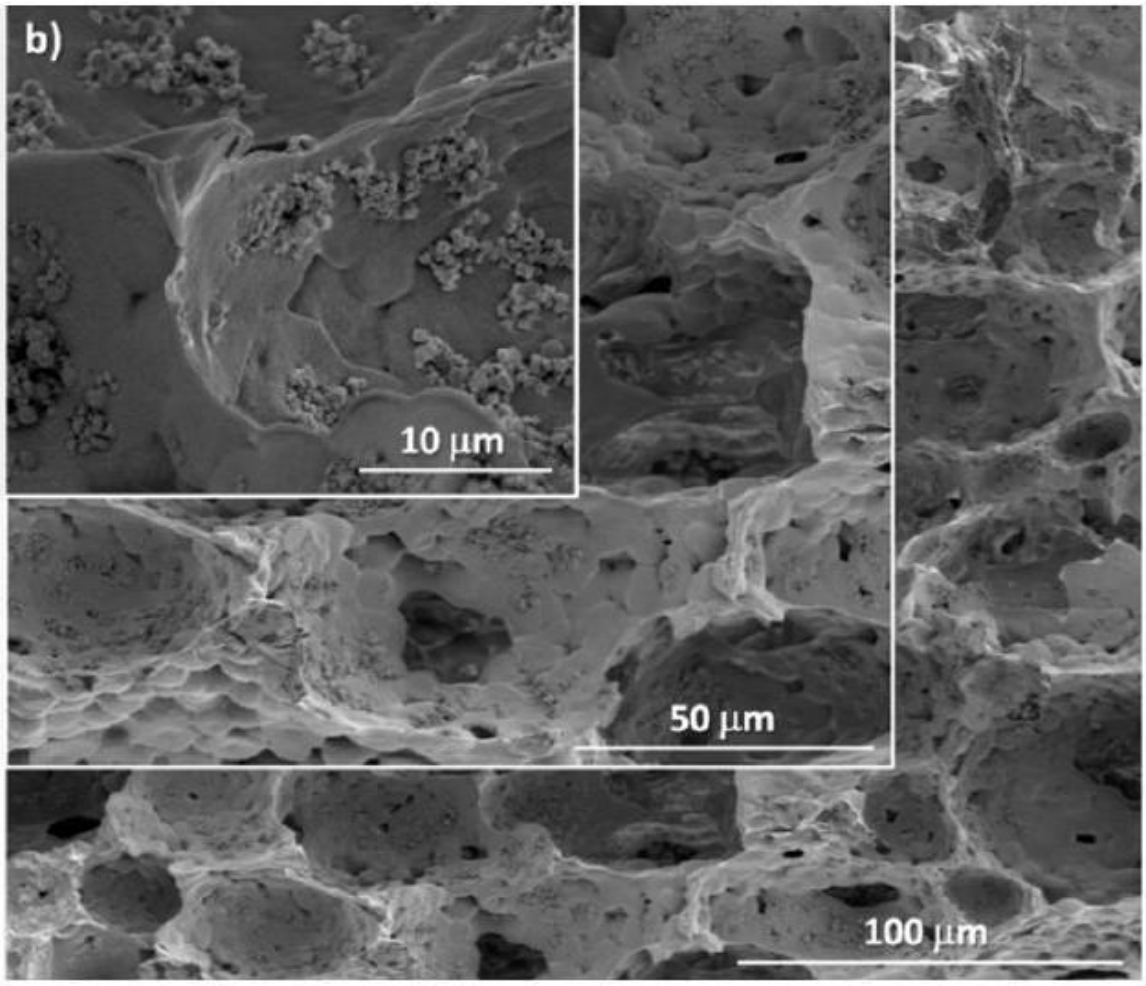

Fig. 7. Cross section SEM images of $BaTiO_3$/P(VDF – TrFE) composites with 16wt% of ceramic particles with filler sizes of a) 10 nm and b) 500 nm .

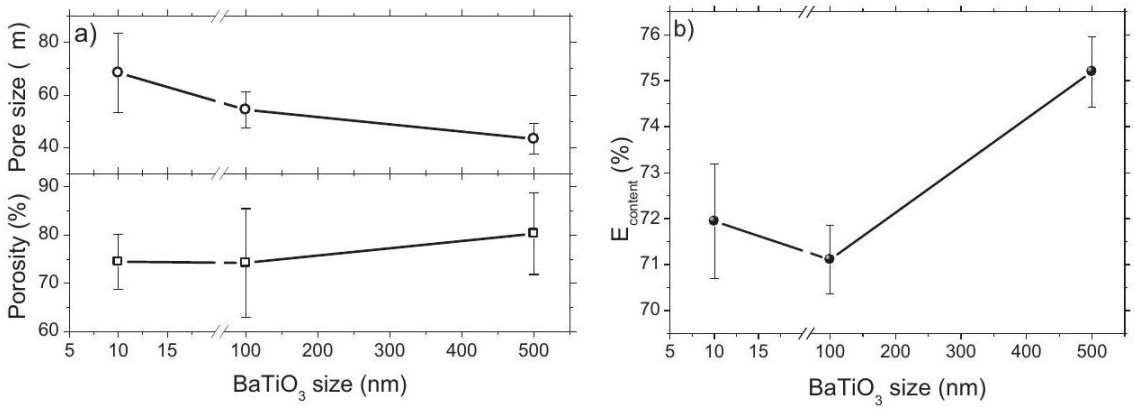

Fig. 8. a) Average pore size and porosity and b) electrolyte content of membranes with 16wt% of $BaTiO_3$ particles as a function of filler average diameter. around 1.0 V and the cathodic peaks around 6.0 V are higher than for lower speeds, since higher scan rates tends induce irreversible electrochemical processes [50]. Generally, the electrochemical stability of the membranes is determined by the electrolyte solution, so the presence of ceramic nanoparticles does not affect significantly the electrochemical behavior. All membranes present a stable operation window at least 5.0 V amplitude, suitable for most common lithium-based couples, which have voltages of about 3.0 V [27]. The diffusion coefficient calculated by eq. 7 through the maximum current value of the oxidative peak in the voltammograms of Fig. 6 shows an increase with increasing $BaTiO_3$ content. The pristine polymer presents the lowest value of 2.85×10^{-5} cm^2/s and the membrane with 32wt% of ceramic nanoparticles presents the highest value of 1.22×10^{-4} cm^2/s, which is similar for the other composites; this effect is attributed to the increase of ionic charge carriers with the addition of fillers.

Particle size effect

In order to study the $BaTiO_3$ filler size effect in the membranes performance, membranes with 16wt% filler content with 10,100 and 500 nm average diameter were prepared. Fig. 8 shows the SEM images for samples with different average filler size.

Fig. 7 show that the different membranes present a homogeneous pore distribution unaffected by the size of the fillers. In all cases the fillers are lodged in the pore cavities, not being incorporated into the polymer matrix structure.

The influence of filler size in pore size, porosity and electrolyte content is presented in Fig. 8.

Concerning to the pore size (Fig. 8a), there is a decrease with increasing filler size, from a maximum of ~ 68 to a minimum of ~ 43μ m for 10 and 500 nm filler average diameter, respectively. During crystallization, the liquid-liquid phase separation of the composite membranes is influenced by ceramic particle size [51], the fillers with larger volume and lower surface area (100 and 500 nm) leading to a decrease of the average pore size.

The porosity (Fig. 8a) and electrolyte content (Fig. 8b), on the other hand, are affected by the size of the fillers. The porosity of the membranes increases and the pore size decreases with increasing ceramic size as shown in Fig. 8a. As the electrolyte content depends on the surface area-to-volume ratio and electrolyte-membrane

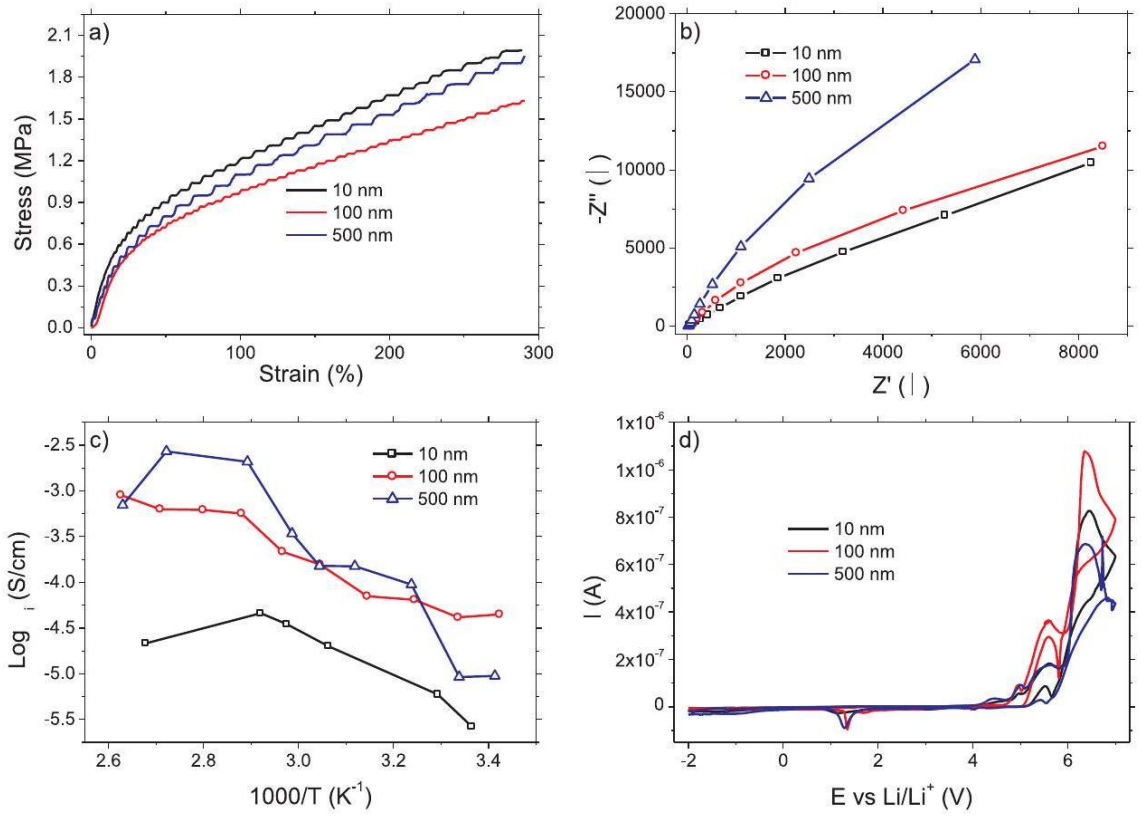

Fig. 9. a) Tensile stress-strain measurements, b) Nyquist plot at 25 °C, c) Log σ as a function of 1000/T and d) cyclic voltammetry, of $BaTiO_3$/P(VDF-TrFE) composites with 16 wt% filler content.

interaction, the electrolyte content increases for increasing ceramic size.

In this sense and despite the differences in pore size, overall porosity and electrolyte uptake are affected by particle size and particle characteristic such as crystalline phase (Table 1).

Fig. 9 presents information about the mechanical and electrical properties of the composite membranes: tensile stress strain, the impedance, ionic conductivity and the electrochemical behavior.

The Fig. 9a shows that the overall mechanical properties are very similar for all composites. The elastic modulus and yield stress are in the same value range for all membranes, 3 – 4 and 0.5 MPa respectively, being nevertheless a dependence on ceramic size due to better wetting due to stronger electrostatic surface interactions of the polymer with the smaller ceramic particles related to the larger surface to volume ratio (Fig. 9a).

In the Nyquist plot of Fig. 9b is notorious the absence of the high frequency semicircle, which also indicates higher ionic mobility for all ceramic size.

The ionic conductivity (Fig. 9c) for a given $BaTiO_3$ concentration is different for each filler average size. Membranes prepared with 500 nm diameter filler particles shows the highest

ionic conductivity, followed by the samples prepared with 100 nm and 10 nm fillers. Therefore, the ionic conductivity of the membranes strongly depends on filler size, increasing with increasing filler average diameter. The 500 nm diameter filler shows ferroelectric properties due to the tetragonal crystallographic form, showing therefore a larger polarity and, in general, ionic conductivity, which in turns leads to higher ionic mobility in the electrolyte [52]. On the other hand, the lowest ionic conductivity is observed for the samples prepared with 10 nm fillers. These are the samples with the larger surface area, leading to increased electrolyte-filler interactions. This fact clearly demonstrate the relevance of filler size on overall membranes performance.

The voltammograms presented in Fig. 9d show that all composite membranes show a stable operation window between - 2.0 and 4.0 V , with a small reduction peak for all samples around 1.0 V .

Overall it can be concluded that filler size is a critical parameter affecting the performance of the membranes for Li-ion battery applications.

Conclusion

$BaTiO_3$/P (VDF-TrFE) porous membranes with different filler contents and sizes were prepared by solvent casting. Filler inclusion leads to an increase in the pore size up to ~ 90μ m and in the porosity up to ~ 74%. The inclusion of the fillers does not influence the phase of the polymer and the ferroelectric-paraelectric and melting temperatures (T_c and T_m) remain unaltered with respect to the values found in the pristine polymer. The main effects of the fillers are a decrease of the degree of crystallinity to 20%, a slight enhancement of the mechanical properties and an increase of the ionic conductivity from 5.24×10^{-7} to 1.04×10^{-4} S/cm for pristine polymer and 4wt% filler content, respectively. The cyclic voltammetry reveals a stable operation window between -2.0 and 4.0 VvsLi/ $Li^+$for all membranes. It is shown that filler size is critical for tailoring membrane properties, higher diameter particles being more effective for increasing electrochemical performance. Furthermore, it was concluded that polymer membranes with 4%wt$BaTiO_3$ ceramic particles with 500 nm average diameter leads to improved battery separator membranes.

Acknowledgements

This work is funded by FEDER funds through the "Programa Operacional Factores de Competitividade-COMPETE" and
by national funds from FCT-Fundação para a Ciência e a Tecnologia, in the framework of the strategic project Strategic Projects PEST-C/FIS/UI607/2011 and PEST-C/QUI/UI0686/2011 and grants SFRH/BD/66930/2009 (J.N.P.) and SFRH/BD/68499/2010 (C.M.C.). The authors thank funding from Matepro-Optimizing Materials and Processes", ref. NORTE-07-0124-FEDER-000037", co-funded by the "Programa Operacional Regional do Norte" (ON.2-O Novo Norte), under the "Quadro de Referência Estratégico Nacional" (QREN), through the "Fundo Europeu de Desenvolvimento

Regional" (FEDER) and support from the COST action MP0902, "Composites of Inorganic Nanotubes and Polymers (COINAPO)".

References

[1] J.-M. Tarascon, Philosophical Transactions of the Royal Society A: Mathematical, Physical and Engineering Sciences 368 (2010) 3227-3241.
[2] J.-K. Park, Principles and applications of lithium secondary batteries, WileyVCH, Weinheim, 2012.
[3] J.M. Tarascon, M. Armand, Nature 414 (2001) 359-367.
[4] D. Linden, T.B. Reddy, Handbook of batteries, McGraw-Hill, New York, 2002.
[5] X. Huang, Journal of Solid State Electrochemistry 15 (2011) 649-662.
[6] P. Arora, Z. Zhang, Chemical Reviews 35 (2004) 4419-4462.
[7] C.M. Costa, J. Nunes-Pereira, L.C. Rodrigues, M.M. Silva, J.L.G. Ribelles, S. Lanceros-Méndez, Electrochimica Acta 88 (2013) 473-476.
[8] S. Ibrahim, S.M.M. Yasin, M.N. Ng, R. Ahmad, M.R. Johan, Solid State Communications 151 (2011) 1828-1832.
[9] L. Persi, F. Croce, B. Scrosati, E. Plichta, M.A. Hendrickson, Journal of The Electrochemical Society 149 (2002) A212-A216.
[10] N. Angulakshmi, K.S. Nahm, J.R. Nair, C. Gerbaldi, R. Bongiovanni, N. Penazzi, A.M. Stephan, Electrochimica Acta 90 (2013) 179-185.
[11] Y. Huai, J. Gao, Z. Deng, J. Suo, Ionics 16 (2010) 603-611.
[12] Y. Liang, Z. Lin, Y. Qiu, X. Zhang, Electrochimica Acta 56 (2011) 6474-6480.
[13] Y.E. Miao, G.N. Zhu, H.Q. Hou, Y.Y. Xia, T.X. Liu, Journal of Power Sources 226 (2013) 82-86.
[14] C.M. Costa, L.C. Rodrigues, V. Sencadas, M.M. Silva, J.G. Rocha, S. LancerosMéndez, Journal of Membrane Science 407-408 (2012) 193-201.
[15] C.M. Costa, V. Sencadas, J.G. Rocha, M.M. Silva, S. Lanceros-Mendez, Journal of Solid State Electrochemistry 17 (2013) 861-870.
[16] C.M. Costa, M.M. Silva, S. Lanceros-Mendez, RSC Advances 3 (2013) 11404-11417.
[17] D. Djian, F. Alloin, S. Martinet, H. Lignier, Journal of Power Sources 187 (2009) 575-580.
[18] X.S. Huang, Journal of Solid State Electrochemistry 17 (2013) 591-597.
[19] J.S. Liu, W.S. Li, X.X. Zuo, S.Q. Liu, Z. Li, Journal of Power Sources 226 (2013) 101-106.
[20] W. Xiao, X. Li, H. Guo, Z. Wang, Y. Zhang, X. Zhang, Electrochimica Acta 85 (2012) 612-621.
[21] J. Nunes-Pereira, A.C. Lopes, C.M. Costa, R. Leones, M.M. Silva, S. LancerosMéndez, Electroanalysis 24 (2012) 2147-2156.
[22] J. Nunes-Pereira, A.C. Lopes, C.M. Costa, L.C. Rodrigues, M.M. Silva, S. Lanceros-Méndez, Journal of Electroanalytical Chemistry 689 (2013) 223232.
[23] P. Martins, A.C. Lopes, S. Lanceros-Mendez, Progress in Polymer Science (2013), http://dx.doi.org/10.1016/j.progpolymsci.2013.07.006.
[24] S. Jung, D. Kim, S. Lee, M. Cheong, D. Nguyen, B. Cho, H. Kim, Polymer 30 (2009) 2355-2361.
[25] M. Moreno, R. Quijada, M.A. Santa Ana, E. Benavente, P. Gomez-Romero, G. González, Electrochimica Acta 58 (2011) 112-118.
[26] L. Lee, S.-J. Park, S. Kim, Solid State Ionics 234 (2013) 19-24.
[27] H.Y. Sun, H.J. Sohn, O. Yamamoto, Y. Takeda, N. Imanishi, Journal of The Electrochemical Society 146 (1999) 1672-1676.
[28] Q. Li, N. Imanishi, Y. Takeda, A. Hirano, O. Yamamoto, Ionics 8 (2002) 79-84.
[29] L.E. Cross, Materials Chemistry and Physics 43 (1996) 108-115.
[30] S. Roberts, Physical Review 71 (1947) 890-895.
[31] D. Damjanovic, F. Brem, N. Setter, Applied Physics Letters 80 (2002) 652654.

[32] H. Mostaghaci, R.J. Brook, J. Mater. Sci. 21 (1986) 3575-3580.
[33] F. Chao, C. Liangyan, Proc. Computer Science and Automation Engineering (CSAE), in: 2012 IEEE International Conference on, 25-27 May 2012, 2012.
[34] I. Nanostructured & Amorphous Materials, Nanostructured & Amorphous Materials, Inc., in, 2001.
[35] S.C. Nunes, V. de Zea Bermudez, D. Ostrovskii, P.B. Tavares, P.C. Barbosa, M.M. Silva, M.J. Smith, Electrochimica Acta 53 (2007) 1466-1475.
[36] D.C. Bassett, Developments in crystalline polymers, Applied Science Publishers, 1982.
[37] A.J. Bard, L.R. Faulkner, Electrochemical Methods: Fundamentals and Applications, Wiley, 2001.
[38] A. California, V.F. Cardoso, C.M. Costa, V. Sencadas, G. Botelho, J.L. GómezRibelles, S. Lanceros-Mendez, European Polymer Journal 47 (2011) 2442-2450.
[39] A. Ferreira, J. Silva, V. Sencadas, J.L.G. Ribelles, S. Lanceros-Méndez, Macromolecular Materials and Engineering 295 (2010) 523-528.
[40] K. Xu, Chemical Reviews 104 (2004) 4303-4418.
[41] A.A. Prabu, J.S. Lee, K.J. Kim, H.S. Lee, Vibrational Spectroscopy 41 (2006) 1-13.
[42] V. Sencadas, S. Lanceros-Méndez, J.F. Mano, Journal of Non-Crystalline Solids 352 (2006) 5376-5381.
[43] C.M. Costa, S. Firmino Mendes, V. Sencadas, A. Ferreira, R. Gregorio Jr., J.L. Gómez Ribelles, S. Lanceros-Méndez, Journal of Non-Crystalline Solids 356 (2010) 2127-2133.
[44] S. Dalle Vacche, F. Oliveira, Y. Leterrier, V. Michaud, D. Damjanovic, J.A.E. Manson, J. Mater. Sci. 47 (2012) 4763-4774.
[45] M. Ulaganathan, R. Nithya, S. Rajendran, Surface Analysis Studies on Polymer Electrolyte Membranes Using Scanning Electron Microscope and Atomic Force Microscope, in: Scanning Electron Microscopy (2012).
[46] B.-Y. Chang, S.-M. Park, Annual Review of Analytical Chemistry 3 (2010) 207-229.
[47] M. Park, X. Zhang, M. Chung, G.B. Less, A.M. Sastry, Journal of Power Sources 195 (2010) 7904-7929.
[48] M. Ulaganathan, S. Rajendran, Soft Materials 8 (2010) 358-369.
[49] D.A. Nissen, Journal of The Electrochemical Society 126 (1979) 176-180.
[50] A.M.C.F.O. Brett, C.M.A. Brett, Electroquímica: princípios, métodos e aplicações, Livraria Almedina, 1996.
[51] K. Nakanishi, N. Soga, Journal of the American Ceramic Society 74 (1991) 2518-2530.
[52] H.-I. Hsiang, F.-S. Yen, Journal of the American Ceramic Society 79 (1996) 1053-1060.